J|A|C|S
ARTICLES
Published on Web 01/17/2003

Shattering of Peptide Ions on Self-Assembled Monolayer Surfaces

Julia Laskin,*,† Thomas H. Bailey,‡ and Jean H. Futrell†

Contribution from the William R. Wiley Environmental Molecular Sciences Laboratory, Pacific Northwest National Laboratory, Post Office Box 999 (K8-96), Richland, Washington 99352, and Department of Chemistry and Biochemistry, University of Delaware, Newark, Delaware 19716

Received July 29, 2002; E-mail: Julia.Laskin@pnl.gov

Abstract: Time- and collision energy-resolved surface-induced dissociation (SID) of des-Arg^1- and des-Arg^9-bradykinin on a fluorinated self-assembled monolayer (SAM) surface was studied by use of a novel Fourier transform ion cyclotron resonance mass spectrometer (FT-ICR MS) specially equipped to perform SID experiments. Time-resolved fragmentation efficiency curves (TFECs) were modeled by an RRKM-based approach developed in our laboratory that utilizes a very flexible analytical expression for the internal energy deposition function capable of reproducing both single- and multiple-collision activation in the gas phase and excitation by collisions with a surface. Both experimental observations and modeling establish a very sharp transition in the dynamics of ion−surface interaction: the shattering transition. The experimental signature for this transition is the appearance of prompt (time-independent) fragmentation, which becomes dominant at high collision energies. Shattering opens a variety of dissociation pathways that are not accessible to slow collisional and thermal ion activation. This results in much better sequence coverage for the singly protonated peptides than dissociation patterns obtained with any of the slow activation methods. Modeling demonstrated that, for short reaction delays, dissociation of these peptides is solely determined by shattering. Internal energies required for shattering transition are approximately the same for des-Arg^1 and des-Arg^9-bradykinin, resulting in the overlap of fragmentation efficiency curves obtained at short reaction delays. At longer delay times, parent ions depletion is mainly determined by a slow decay rate and fragmentation efficiency curves for des-Arg^1 and des-Arg^9-bradykinin diverge. Dissociation thresholds of 1.17 and 1.09 eV and activation entropies of −22.2 and −23.3 cal/(mol K) were obtained for des-Arg^1 and des-Arg^9-bradykinin from RRKM modeling of time-resolved data. Dissociation parameters for des-Arg^1-bradykinin are in good agreement with parameters derived from thermal experiments. However, there is a significant discrepancy between the thermal data and dissociation parameters for des-Arg^9-bradykinin obtained in this study. The difference is attributed to the differences in conformations that undergo thermal activation and activation by ion−surface collisions prior to dissociation.

Introduction

Ion−surface impact is a fast and efficient means of excitation of large molecules, for which deposition of energy into vibrational modes of the projectile molecule occurs on a time scale of a few picoseconds. Competing physical and chemical processes occurring during collisions of low-energy (1−100 eV) polyatomic ions with different surfaces have been recently reviewed.[1] These include neutralization or soft landing of ions, surface modification and chemical sputtering of the surface material, scattering, and surface-induced dissociation (SID) of projectile ions. Relative yields of these processes are largely determined by the physical properties of the surface. Self-assembled monolayers (SAMs) of fluorinated thiols on gold substrates are excellent targets for SID because of the reduced neutralization efficiency compared to metal surfaces and the relatively high efficiency of internal excitation of ions that is easily achieved.[2,3] The latter is an important prerequisite for effecting fragmentation of large ions because dissociation rate constants of complex molecules decrease dramatically with an increase in the number of vibrational degrees of freedom.

In the past decade, several groups have utilized SID as an effective tool for structural characterization of protonated peptides and proteins.[3−8] It was found that in many cases ion−surface impact results in extensive fragmentation of peptide ions. Similarly to low-energy collision-induced dissociation (CID)

* Corresponding author: fax (509) 376-3650.
† Pacific Northwest National Laboratory.
‡ University of Delaware.

(1) Grill, V., Shen, J.; Evans, C.; Cooks, R. G. *Rev. Sci. Instrum.* **2001**, *72*, 3149.
(2) Cooks, R. G.; Ast, T.; Pradeep, T. *Acc. Chem. Res.*, **1994**, *27*, 316.
(3) Dongré, A. R.; Somogyi, A.; Wysocki, V. H. *J. Mass Spectrom.* **1996**, *31*, 339.
(4) McCormack, A. L.; Somogyi, Á.; Dongré, A. R.; Wysocki, V. H. *Anal. Chem.*, **1993**, *65*, 2859.
(5) Laskin, J.; Denisov, E.; Futrell, J. H. *J. Am. Chem. Soc.* **2000**, *122*, 9703.
(6) Laskin, J.; Denisov, E.; Futrell, J. H. *J. Phys. Chem. B* **2001**, *105*, 1895.
(7) Stone, E.; Gillig, E.; Ruotolo, B.; Fuhrer, K.; Gonin, M.; Schultz, A.; Russell, D. H. *Anal. Chem.* **2001**, *73*, 2233.
(8) Mohammed, S.; Chalmers, M. J.; Gielbert, J.; Ferro, M.; Gora, L.; Smith, D. C.; Gaskell, S. J. *J. Mass Spectrom.* **2001**, *36*, 1260.

SID results in formation of a, b, and y ions originating from backbone cleavages as well as internal fragments. However, at sufficiently high collision energies some side-chain-specific fragments characteristic of high-energy CID, such as d and w ions, are observed.[3] The type and amount of fragments in SID spectra depend on the energetics and mechanisms of peptide fragmentation, reaction time sampled by the instrument, internal energy distribution of excited ions, and the detailed dynamics of ion−surface interaction.

Extensive studies on interaction of small peptides with fluorinated SAMs and gas-phase collisional activation conducted in our laboratory demonstrated that both methods of collisional activation produce vibrationally excited ions with quasi-thermal distributions of internal energies.[6,9] Consequently, low-energy CID and SID mass spectra of small peptides are very similar. However, this is not the case for large peptides, which require fairly high collision energy for fragmentation.[10] For large peptides, low-energy CID spectra remain dominated by backbone fragmentation, while SID spectra obtained at different collision energies contain mainly low-mass fragments and are similar to high-energy CID spectra.[4,10] It has been suggested that this difference between low-energy CID and SID spectra of large peptides is a result of a longer observation time of trapping instruments that are commonly utilized for low-energy multiple-collision CID studies (MCA-CID) as compared to typical SID instruments, which sample fragmentation occurring on a microsecond time scale.[11] In this study SID is coupled with Fourier transform ion cyclotron resonance mass spectrometry (FT-ICR MS). This allows sampling of much longer reaction times (from hundreds of microseconds to many seconds) and conduct of kinetics studies to investigate the time dependence of peptide fragmentation. Moreover, long observation time reduces the kinetic shift (i.e., the amount of excess internal energy required to observe fragmentation) and enables the observation of dissociation at significantly lower collision energies than sector instruments.

Dissociation of large peptides into many small fragments observed in SID studies utilizing tandem-quadrupole instruments can also be explained by a change in the dynamics of ion−surface interaction occurring in the range of collision energies sampled experimentally. For example, it has been observed experimentally that the fragmentation pattern of fullerenes undergoes a sharp transition from the low-energy regime characterized by sequential evaporation of C_2 units from fullerene cages to the high-energy regime characterized by formation of small even- and odd-numbered carbon clusters.[12] A similar transition was observed for other cluster ions[13−15] and small molecules[16] and attributed to the transition from recoil to shattering of cluster ions on surfaces.[17,18] In this case ions undergo fragmentation at the surface rather than in the gas phase. The maximum entropy method was applied to simulate fragmentation patterns of C_{60}, in excellent agreement with experimental observations.[19]

Hase and co-workers[20,21] have studied the dynamics of interaction of $Cr(CO)_6^+$ and small polyglycines with *n*-hexylthiolate SAM and diamond surface using classical trajectory simulations and harmonic potential energy surface for the projectile ion, which does not allow fragmentation. These simulation provided very interesting information on the efficiency of energy transfer in ion−surface collisions and its dependence on both the structure of projectile ion and physical properties of the surface. However, "nonreactive" simulations cannot be used to predict fragment distributions. Furthermore, including reactive potential energy surfaces for peptide ions in these simulations is challenging. This has been done recently for the case of protonated glycine colliding with a hydrogenated diamond {111} surface.[22] It was found that, at a collision energy of 70 eV, 55% of dissociation results from shattering, i.e., fragmentation occurs while protonated glycine collides with a surface.

Shattering of ions on surfaces can be identified by measuring velocity or kinetic energy distributions of their fragments.[16] It has been demonstrated that fragment ions formed in the gas phase have similar velocity distributions, while fragment ions produced directly on the surface via a shattering mechanism are expected to have similar kinetic energies and different velocities.[16] Hanley and co-workers[23] reported velocity distributions of several small peptide ions and their fragments produced by collisions with hexanethiolate SAMs. It was found that in the range of collision energies from 15 to 55 eV all fragments had the same velocity distributions, which was attributed to the unimolecular fragmentation of precursor ions following their recoil from the surface.

In this study we present the first experimental evidence for shattering of peptide ions on fluorinated SAMs by following fragmentation behavior of two octapeptides: protonated des-Arg^1- and des-Arg^9-bradykinins (PPGFSPFR and RPPGFSPF). Coupling SID with FT-ICR MS allowed us to distinguish between the effect of observation time window and transition in the dynamics of peptide ion−surface interaction on fragmentation patterns of protonated peptides.

Experimental Section

Mass Spectrometry. Surface-induced dissociation experiments were conducted on a specially fabricated 6T FT-ICR mass spectrometer. The instrument is equipped with a high-transmission electrospray source, consisting of an ion funnel interface[24] followed by three quadrupoles. The instrument is also fitted with a vacuum interlock assembly that allows the SID target to be positioned just inside the rear trapping plate of the ICR cell. Both the instrument and SID experimental protocol have been detailed elsewhere[25] and will be only briefly outlined below.

(9) Laskin, J.; Futrell, J. H. *J. Chem. Phys.* **2002**, *116*, 4302.
(10) Zhong, W. Ph.D. Thesis, Virginia Commonwealth University, 1999.
(11) Tsaprailis, G.; Nair, H.; Somogyi, A.; Wysocki, V. H.; Zhong, W.; Futrell, J. H.; Summerfield, S. G.; Gaskell, S. J. *J. Am. Chem. Soc.* **1999**, *121*, 5142.
(12) Beck, R. D.; Warth, C.; May, K.; Kappes, M. M. *Chem. Phys. Lett.* **1996**, *257*, 557.
(13) Hendell, E.; Even, U.; Raz, T.; Levine, R. D. *Phys. Rev. Lett.* **1995**, *75*, 2670.
(14) Cristen, W.; Even, U.; Raz, T.; Levine, R. D. *Int. J. Mass Spectrom. Ion Processes* **1998**, *174*, 35.
(15) Kaiser, B.; Bernhardt, T. M.; Stegemann, B.; Opitz, J.; Rademann, K. *Phys. Rev. Lett.* **1999**, *83*, 2918.
(16) Schultz, D. G.; Hanley, L *J. Chem. Phys.* **1998**, *109*, 10976.
(17) Raz, T.; Even, U.; Levine, R. D. *J. Chem. Phys.* **1995**, *103*, 5394.
(18) Raz, T.; Levine, R. D. *J. Chem. Phys.* **1996**, *105*, 8097.
(19) Campbell, E. E. B.; Raz, T.; Levine, R. D. *Chem. Phys. Lett.* **1996**, *253*, 261.
(20) Bosio, S. B. M.; Hase, W. L. *Int. J. Mass Spectrom.* **1998**, *174*, 1.
(21) Meroueh, O.; Hase, W. L. *J. Am. Chem. Soc.* **2002**, *124*1, 1524.
(22) Meroueh, O.; Wang, Y.; Hase, W. L. *J. Phys. Chem. A* **2002**, *106*, 9983.
(23) Schultz, D. G.; Lim, H.; Garbis, S.; Hanley, L. *J. Mass Spectrom.* **1999**, *34*, 217.
(24) Shaffer, S. A.; Tang, K.; Anderson, G. A.; Prior, D. C.; Udseth, H. R.; Smith, R. D. *Rapid Commun. Mass Spectrom.* **1997**, *11*, 1813.
(25) Laskin, J.; Denisov, E. V.; Shukla, A. K.; Barlow, S. E.; Futrell, J. H. *Anal. Chem.* **2002**, *74*, 3255.

The self-assembled monolayer (SAM) surface was prepared on a single gold crystal (Monocrystals, Richmond Heights, OH) by a standard procedure. The target was cleaned in a UV cleaner (Model 135500, Boekel Industries Inc., Feasterville, PA) for 10 min and allowed to stand in a 1 mM ethanol solution of FC_{12} [$CF_3(CF_2)_9C_2H_4SH$] for 24−36 h. The target was removed from the SAM solution and ultrasonically washed in ethanol for 10 min to remove extra layers. Immediately after washing, the SAM surface is positioned on the end of an insertion probe and is inserted into the ultrahigh vacuum region of the FT-ICR, through a vacuum interlock at the rear of the instrument. The surface is positioned 1−2 mm inside of the rear trapping plate of the ICR cell. The surface is electrically connected to the rear trapping plate power supply. This ensures that the SAM surface and the rear trapping plate are at the same potential throughout the experiment.

Ions are electrosprayed, at atmospheric pressure, into the end of a heated stainless steel capillary tube. The ions travel through the capillary tube, into the vacuum system, and into the entrance of the ion funnel. The ion funnel provides highly efficient ion transfer into the high vacuum region of the mass spectrometer. The first quadrupole, immediately following the ion funnel, collisionally cools the ions exiting the ion funnel. Upon exiting the first quadrupole, the parent ion of interest (singly protonated ions in all of the following experiments) is mass-selected in the second quadrupole and accumulated in the third quadrupole for 0.3−0.8 s. The third (accumulation) quadrupole is held at an elevated pressure (2×10^{-3} Torr) for collisional relaxation of stored ions. Collisional relaxation is necessary to ensure efficient thermalization of the parent ion population.

After accumulation, the ions are extracted from the third quadrupole with an extraction pulse 250 ms wide (ion accumulation and ejection are controlled by applying the necessary voltages to apertures positioned on either side of quadrupole three). Following ion ejection, a time-of-flight (TOF) delay allows the ions time to fly through the transfer optics to the ICR cell where they collide with the surface. The TOF delay is typically 80−140 ms, depending on the parent ion mass. Scattered ions are captured by raising the potentials on the front and rear trapping plates of the ICR cell by 10−15 V. Time-resolved mass spectra were acquired by varying the delay between the gated trapping and the excitation/detection event (the reaction delay). Typically, the reaction delay was varied from 1 ms to 1 s. Immediately following the fragmentation delay, ions were excited by a broadband chirp and detected.

The collision energy is defined by the difference in the potential applied to the accumulation quadrupole and the potential applied to the rear trapping plate and the SID target. The ICR cell can be offset above or below ground by as much as ±150 V. Lowering the ICR cell below ground while keeping the potential on the third quadrupole fixed increases collision energy for positive ions. Because the translational energy of the ion is changed within the constant high magnetic field region of the ICR, ion transmission characteristics of the instrument remain the same at all collision energies. Consequently parent ion currents and ion trajectories are constant and independent of collision energy.[25]

Experimental control is accomplished with a MIDAS data station.[26] MIDAS is used to control the voltages and timing of the source and transfer optics as well as the excite/detect events in the ICR cell. An automated script was written to allow for unattended acquisition of kinetic data. The script was used to vary the fragmentation delay and collision energy of the experiment. Reactions delays of 1 ms, 10 ms, 50 ms, 0.1 s, 0.3 s, and 1 s were studied. Typical experiments involved changing the collision energy across a relatively wide range from 8 to 48 eV. The automated script allowed for acquisition of SID spectra across the entire range of collision energies, in 1 eV increments, at each of the six fragmentation delays. Time-dependent fragmentation efficiency curves (TFECs) were constructed from experimental mass spectra by plotting the relative intensity of the precursor ion as a function of collision energy for each fragmentation delay.

Des-Arg^1- and des-Arg^9-bradykinin were purchased from Sigma and used as received. All samples were dissolved in a 50/50 (v/v) methanol/water solution with 1% acetic acid. A syringe pump (Cole Parmer, Vernon Hills, IL) was used for direct infusion of the electrospray samples at flow rates ranging from 20 to 50 μL/h.

RRKM Modeling. The TFECs were modeled using an RRKM-based approach as described previously:[5,27,28]

(1) The microcanonical rate coefficient $k(E)$ is calculated as a function of internal energy by use of the microcanonical RRKM/QET expression:

$$k(E) = \frac{\sigma W^{\ddagger}(E - E_0)}{h\rho(E)} \tag{1}$$

where $\rho(E)$ is the density of states of the reactant, $W^{\ddagger}(E - E_0)$ is the sum of states of the transition state, E_0 is the critical energy, h is Planck's constant, and σ is the reaction path degeneracy.

(2) The survival probability of the parent ion and the probability for the formation of fragment ions as a function of the internal energy of the parent ion and the experimental observation time (t_r), $F_i(E, t_r)$, were calculated from the rate−energy $k(E)$ dependency, taking into account radiative decay of the excited ion population. The function $F_i(E, t_r)$ is commonly referred to as a breakdown curve. A collection of breakdown curves, called the breakdown graph (BDG), was then constructed from the individual breakdown curves calculated for each reaction channel.

(3) The internal energy deposition function was described by the following analytical expression:

$$P(E,E_{\text{coll}}) = \frac{1}{C}(E - \Delta)^l \exp\left(-\frac{(E - \Delta)}{f(E_{\text{coll}})}\right) \tag{2}$$

where l and Δ are parameters, $C = \Gamma(l + 1)[f(E_{\text{coll}})]^{l+1}$ is a normalization factor, and $f(E_{\text{coll}})$ has the form

$$f(E_{\text{coll}}) = A_2E_{\text{coll}}^{\ 2} + A_1E_{\text{coll}} + A_0 \tag{3}$$

where A_0, A_1, and A_2 are parameters and E_{coll} is the collision energy.

We have shown previously that the proposed analytical form for the collisional energy deposition function has enough flexibility to reproduce experimental fragmentation efficiency curves obtained from both gas-phase collisional activation and SID.[5,6,9,27,28] An exponential function obtained with $l = 0$ can be used to model single-collision CID experiments, while a Boltzmann-like function (high values of l) has been utilized to reproduce multiple-collision CID and SID data.

(4) Collisional activation produces ions with a wide distribution of internal energies, $P(E, E_{\text{CM}})$. The contribution of ions having internal energy E to the observed signal intensity for a particular reaction channel i equals $F_i(E, t_r)P(E, E_{\text{CM}})$. Integrating over internal energies yields an overall signal intensity at a given center-of-mass (CM) collision energy, $I(E_{\text{CM}})$:

$$I_i(E_{\text{coll}}) = \int_0^{\infty} F_i(E, t)P(E, E_{\text{coll}})\, dE \tag{4}$$

Vibrational frequencies for the precursor ions were adopted from our previous study.[29] Vibrational frequencies for the transition state were estimated by removing one C−N stretch (reaction coordinate)

(26) Senko, M. W.; Canterbury, J. D.; Guan, S.; Marshall, A. G. *Rapid Commun. Mass Spectrom.* **1996**, *10*, 1839.
(27) Laskin, J.; Byrd, M.; Futrell, J. H. *Int. J. Mass Spectrom.* **2000**, *195/196*, 285.
(28) Laskin, J.; Futrell, J. H. *J. Phys. Chem. A* **2000**, *104*, 5484−5494.
(29) Laskin, J.; Bailey, T. H.; Denisov, E. V.; Futrell, J. H. *J. Phys. Chem. A* **2002**, *106*, 9832.

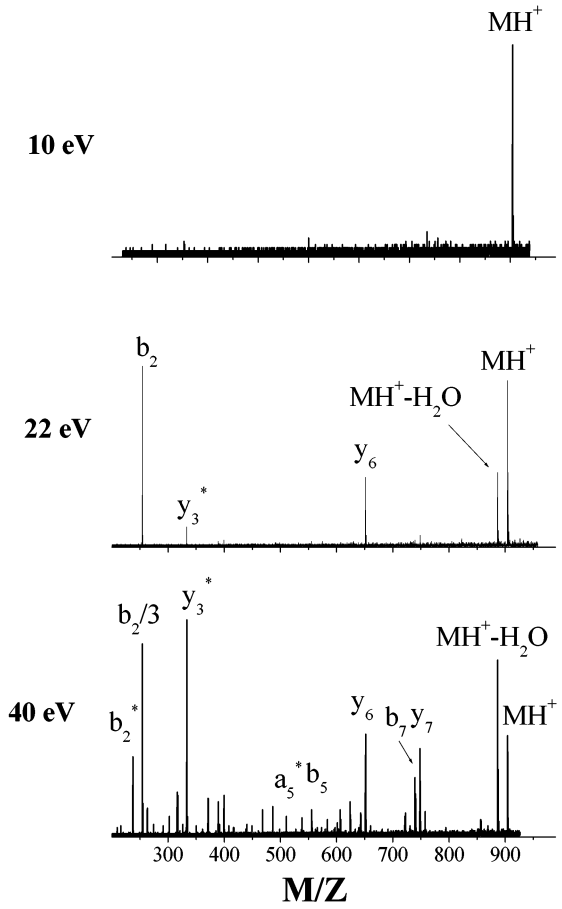

Figure 1. SID mass spectra of des-Arg^9-bradykinin at collision energies of 10, 22, and 40 eV and 1 s reaction delay.

from the parent ion frequencies as well as varying 15 frequencies in the range of 300−1500 cm^{-1} to obtain the best fit with experimental data.

TFECs were constructed by the above procedure and compared to experimental data. The internal energy deposition function was kept the same for all reaction times. The fitting parameters included the critical energy and activation entropy for dissociation of the precursor ion and parameters characterizing the energy deposition function (eqs 2 and 3). They were varied until the best fit to experimental fragmentation efficiency curves was obtained. The uniqueness of the fits was confirmed by sensitivity analysis described elsewhere.[5,28]

Results and Discussion

Fragmentation Behavior of des-Arg^1 and des-Arg^9-Bradykinin. Figure 1 shows SID spectra of des-Arg^9-bradykinin at 10, 22, and 40 eV for 1 s fragmentation delay. At low collision energies, fragmentation spectra of both des-Arg^1-bradykinin (PPGFSPFR) and des-Arg^9-bradykinin (RPPGFSPF) are very similar to BIRD spectra obtained by FT-ICR MS.[30] Very few fragment ions are observed at low collision energies for both precursor ions. The major low-energy fragmentation pathways for des-Arg^9-bradykinin correspond to loss of water and formation of b_2 and y_6 ions. We refer to the low-energy fragments as to the primary fragments. The $y_3 - NH_3$ ion (not observed in BIRD spectra) has a somewhat higher dissociation threshold than the three major low-energy product ions. Water loss and formation of y_6 ion are the major primary fragments

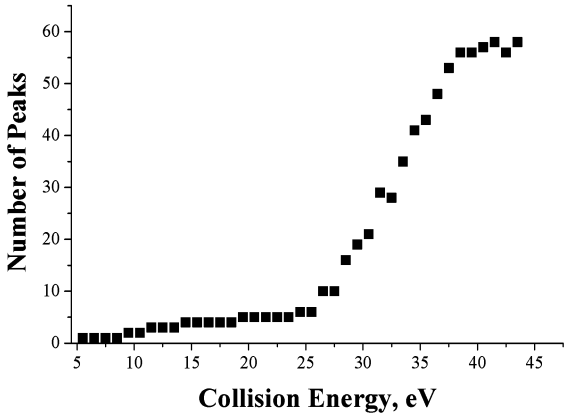

Figure 2. Number of peaks in SID spectrum of des-Arg^9-bradykinin as a function of collision energy for 1 s reaction delay.

of des-Arg^1-bradykinin (spectra not shown). A higher-energy pathway for des-Arg^1-bradykinin results in formation of b_7 + OH ion, a typical rearrangement fragment for arginine-containing peptides.[31,32]

At higher collision energies the amount of fragment ions in SID spectra of both peptides increases dramatically. These include both high and low mass ions and display good sequence coverage as compared to the poor fragmentation observed at lower collision energies. Figure 2 shows the increase in the number of peaks in the spectrum (number of spectral features above the noise level) as a function of collision energy for des-Arg^9-bradykinin. Similar results (not shown) were obtained for des-Arg^1-bradykinin. Obviously, there is a fairly wide range of collision energies (10−30 eV), for which SID spectra contain only few fragment ions. However, at collision energies above 30 eV the curve in Figure 2 shows a very sharp increase. A 5 eV increase in collision energy from 32 to 37 eV results in a 10-fold increase in the number of fragment ions. Interestingly, only part of these fragments can be accounted for by the assumption of consecutive dissociation of the primary product ions, meaning that most of the high-energy fragments are formed directly from the protonated precursor. This assertion was further confirmed by time-resolved studies described in the following section.

Time-Resolved Studies. Combination of SID with FT-ICR MS facilitates kinetics studies of ion dissociation following activation by surface impact as a function of fragmentation delay times ranging from hundreds of microseconds to several seconds. Time-resolved fragmentation efficiency curves (TFECs) for the precursor ion and its fragments are obtained by varying ion collision energy and reaction time and plotting the relative abundance of each ion as a function of collision energy for each fragmentation delay. In this study we obtained TFECs for des-Arg^1- and des-Arg^9-bradykinin with reactions delays of 1 ms, 10 ms, 50 ms, 0.1 s, 0.3 s, and 1 s. Typical results obtained for des-Arg^9-bradykinin and its selected fragment ions are shown in Figure 3. Fragmentation efficiency curves for the precursor ion and all primary fragments are strongly dependent on the reaction time, while the curves for most of the high-energy fragments do not show any time dependence. Obviously, the

(30) Schnier, P. D.; Price, W. D.; Jockusch, R. A.; Williams, E. R. *J. Am. Chem. Soc.* **1996**, *118*, 7178.
(31) Thorne, G. C.; Ballard, K. D.; Gaskell, S. J. *J. Am. Soc. Mass Spectrom.* **1990**, *1*, 249.
(32) Vachet, R. W.; Asam, M. R.; Glish, G. L. *J. Am. Chem. Soc.* **1996**, *118*, 6252.

time-independent fragments are formed by a fast fragmentation of the excited precursor ion and not by consecutive dissociation of the primary fragments. We interpret the time-independent, prompt dissociation of ions as resulting from shattering of the primary ion at higher collision energy.

For protonated des-Arg^9-bradykinin about half of the fragment ions exhibit some time dependence, with the most pronounced time dependence displayed by the primary fragments listed above. In contrast, only four time-dependent fragments were observed for protonated des-Arg^1-bradykinin precursor ion: $MH^+ - H_2O$, y_6, $b_7 + OH$, and $b_5 - H_2O$. The most abundant time-independent fragment of des-Arg^1-bradykinin is the y_1 ion. Other time-independent fragments correspond to backbone fragmentation of the precursor ion and can be readily identified. Most of the internal fragments do not exhibit any time dependence. It should be noted, however, that the same internal fragments produced from the two different isomer precursor ions do not necessarily display the same dependence on the reaction time. For example, the curve for the GFS $- H_2O$ fragment (*m*/*z* 274) is time-independent for both bradykinins, while the PGFS ion (*m*/*z* 389) is time-dependent when des-Arg^9-bradykinin is the precursor ion and does not depend on time when des-Arg^1-bradykinin is the precursor ion.

Modeling of Experimental TFECs. RRKM modeling as outlined above was utilized to obtain decomposition rates for protonated des-Arg^1- and des-Arg^9-bradykinin. For the modeling we separated time-dependent and time-independent fragments and used two dissociation rate constants for the total ion decomposition to account for the slow and fast fragmentation, as indicated schematically below.

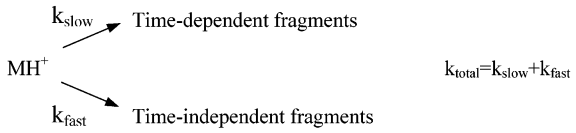

Microcanonical rate constants as a function of internal energy for the slow channel were calculated by the RRKM expression. For the fast reaction pathway we found that the rate−energy dependence is very sharp and is best described by a step function originating from the assumed threshold energy. Breakdown curves were calculated for the precursor ion and both time-dependent and time-independent fragments by use of the rate−energy dependencies. Radiative decay rate was assumed to be independent of the internal energy. This approximation is justified because radiative rates exhibit a very slow dependence on the internal energy of the ion as compared to fragmentation rates, which allows use of a single value for the radiative decay rate representing an average over a range of internal energies.

Modeling results were obtained by simultaneously fitting the TFECs of the precursor ion and the time-dependent and time-independent fragments. The results for des-Arg^1-bradykinin are shown in Figure 4. Symbols represent experimental points obtained at fragmentation delays of 1 ms, 10 ms, 100 ms, and 1 s, while modeling results are shown as solid lines. There is a good agreement between experimental and simulated results. The corresponding dissociation parameters are summarized in Table 1. Dashed lines in Figure 4a were obtained by blocking the fast fragmentation channel. These lines represent the relative contribution of the slow fragmentation to the parent ion TFECs.

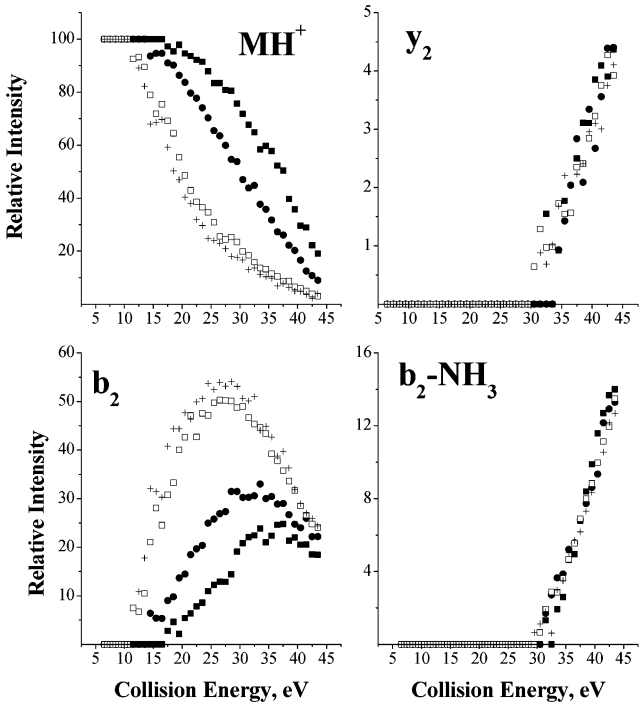

Figure 3. Time- and energy-resolved FECs for the parent ion and selected fragments of des-Arg^9-bradykinin for reaction delays of 1 ms (■), 10 ms (●), 100 ms (□), and 1 s (+).

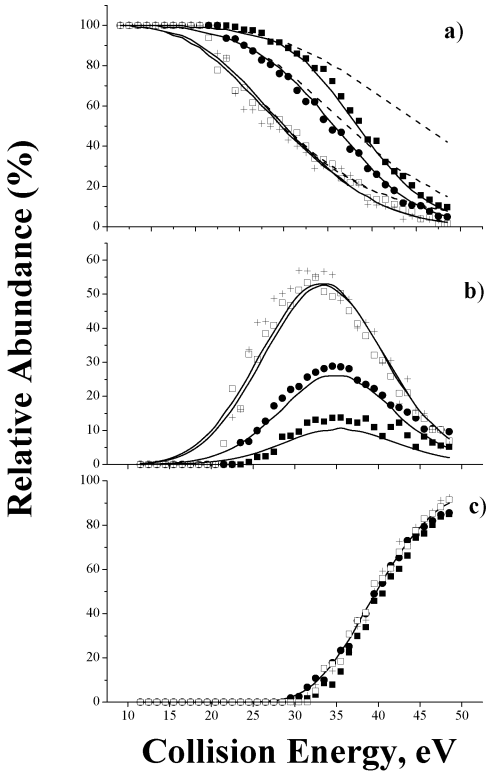

Figure 4. Experimental FECs for (a) the parent ion, (b) time-dependent fragments, and (c) time-independent fragments of des-Arg^1-bradykinin for reaction delays of 1 ms (■), 10 ms (●), 100 ms (□), and 1 s (+). Solid lines represent the modeling results, taking into account slow and fast dissociation channels (see text for details). Dashed lines in panel (a) represent the contribution of the slow decay channel to the FEC of the parent ion.

Clearly, for long reaction delays the parent ion depletion is caused mainly by slow dissociation, while the contribution of

Table 1. Threshold Energies and Transition-State Entropies

	RPPGFSPF (des-Arg^9-bradykinin)	PPGFSPFR (des-Arg^1-bradykinin)
	From SID Data (this work)	
E_{slow}, eV	1.09 ± 0.03	1.17 ± 0.03
$\Delta S^{\ddagger}$,[a] e.u.	-23.3 ± 0.7	-22.2 ± 0.7
A,[b] s^{-1}	2×10^8	4×10^8
E_{fast}, eV	9.5 ± 0.5	9.2 ± 0.5
% T → V	19.5 ± 1.5	18.8 ± 1.5
	From BIRD Data[c]	
E_a, eV	1.2	0.82
A, s^{-1}	10^{12}	10^7
E_0,[d] eV	1.24	1.15
$\Delta S^{\ddagger}$,[d] e.u.	−6.4	−29.4

[a] Entropy units (e.u.) = calories (mole Kelvin)$^{-1}$. [b] Calculated from $\Delta S^{\ddagger}$ assuming a temperature of 450 K. [c] Reference 30. [d] Reference 29.

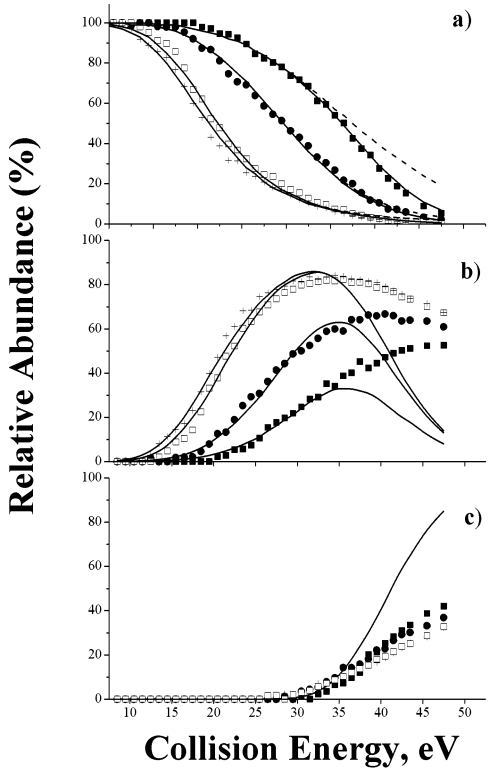

Figure 5. Same as in Figure 4 but for des-Arg^9-bradykinin.

the fast fragmentation pathway becomes dominant at shorter delays.

Experimental and simulated TFECs for des-Arg^9-bradykinin are compared in Figure 5. There is excellent agreement between experimental and calculated curves for the precursor ion. However, for this ion, modeling of time-dependent and time-independent fragments in a wide range of collision energies was not successful. Obviously, for des-Arg^9-bradykinin part of the fragment ions are formed both by slow unimolecular decay at low collision energies and by fast decay at high collision energies. Because we cannot distinguish between the fast and slow component within the same experimental fragmentation efficiency curve, we overestimate the amount of time-dependent fragments and underestimate the amount of time-independent fragments at high collision energies. This is clearly indicated by our modeling results.

Shattering Transition. Interestingly, we found that decomposition rates for the fast reaction channel are well represented

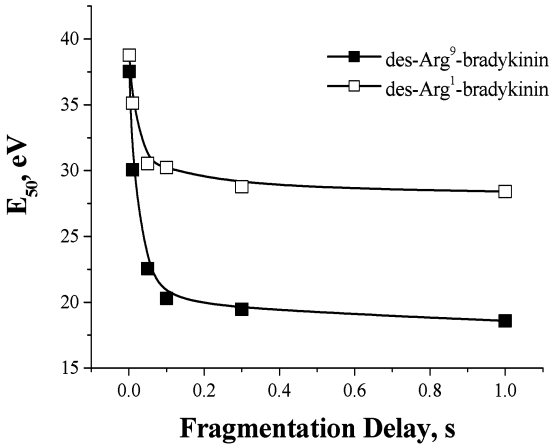

Figure 6. Time dependence of the collision energy required to obtain 50% dissociation of the precursor ion for des-Arg^1- and des-Arg^9-bradykinin. Lines are shown to guide the eye.

by the sudden death approximation, i.e., assuming that the precursor ion with internal energy above a certain threshold fragments instantly. This is quite unexpected for unimolecular dissociation of ions of this size. We suggest that opening of a fast fragmentation pathway is indicative of the transition from recoil of precursor ions from the surface followed by slow unimolecular decay in the gas phase to shattering of ions on the surface. It was mentioned earlier that this transition has been previously observed for cluster ions[12−19] and for the protonated glycine.[22] The transition occurs as a result of a very fast heating of ions above a certain internal energy by ion−surface collision. The internal excitation required for opening of the fast dissociation pathway is 9.2 ± 0.5 eV for des-Arg^1-bradykinin and 9.5 ± 0.5 eV for des-Arg^9-bradykinin.

The contribution of shattering to the decay of the precursor ion is more pronounced at higher collision energies and shorter reaction times. In our previous study, which emphasized only the slow fragmentation path, we predicted that fragmentation efficiency curves for the two precursor ions should significantly diverge from each other at short reaction times, with the curve for des-Arg^9-bradykinin appearing at lower collision energy.[29] This result was in apparent contradiction with collision energy-resolved SID data for these ions reported by Wysocki and coworkers,[33] which demonstrated that on a microsecond time scale the collision energies required in order to obtain 50% fragmentation (E_{50}) of des-Arg^1- and des-Arg^9-bradykinin are essentially the same (78.8 and 78.3 eV, respectively). We suggested that this discrepancy was evidence for a change in the mechanism of ion−surface interaction at high collision energies sampled in the tandem-quadrupole experiments.

Time dependence of E_{50} for both precursor ions obtained in this study is shown in Figure 6. Obviously, the values of E_{50} are significantly different at longer reaction times and become very close at 1 ms. The shapes of experimental TFECs obtained at 1 ms and 1 s, shown in Figure 7, are quite different: TFECs become sharper at shorter reaction times. Simulated curves for 10 μs reaction time for des-Arg^1- and des-Arg^9-bradykinin perfectly overlap, which is in excellent agreement with SID results from tandem-quadrupole instrument.[33] However, our simulations show that parent ion decay at 10 μs results solely

(33) Dongré, A. R.; Jones, J. L.; Somogyi, Á.; Wysocki, V. H. *J. Am. Chem. Soc.* **1996**, *118*, 8365.

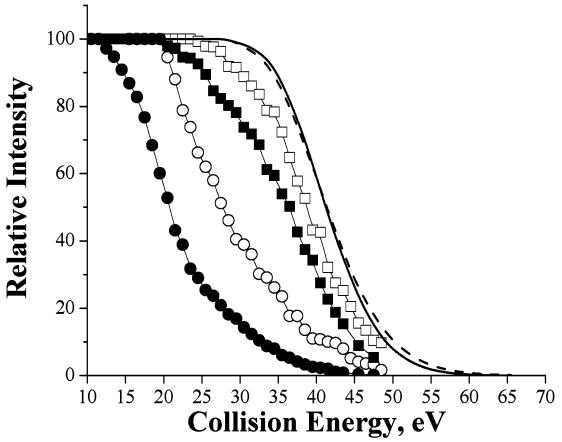

Figure 7. FECs for des-Arg^1- (open symbols) and des-Arg^9-bradykinin (filled symbols) at 1 ms (squares) and 1 s (circles) reaction delay. Solid and dashed lines represent simulated curves at 10 μs reaction time for des-Arg^9- and des-Arg^1-bradykinin, respectively.

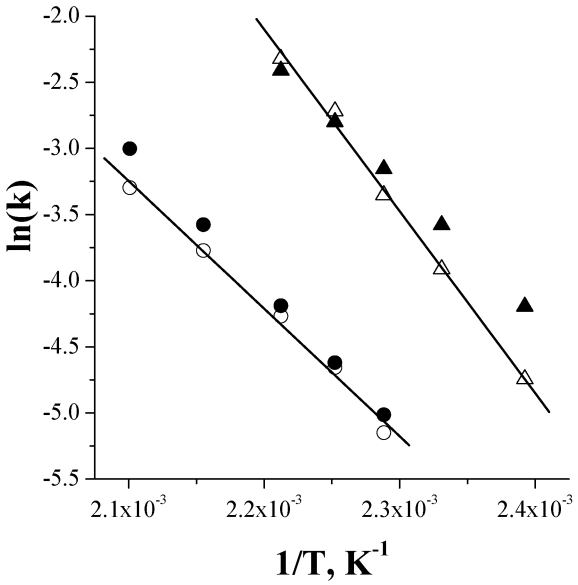

Figure 8. Arrhenius plot reported in ref 30 (open symbols and lines) together with thermal rate constants obtained by averaging microcanonical rate−energy dependencies over thermal distributions at the same temperatures (filled symbols) for des-Arg^1- (circles) and des-Arg^9-bradykinin (triangles).

from shattering, i.e., represents only the fast decay rate. It is also obvious that convergence of TFECs and E_{50} at short reaction times is a direct consequence of the shattering transition, which makes fast decay dominant at short reaction times. Sharp dependence of the fragmentation efficiency on collision energy was previously attributed to the narrow internal energy distribution deposited into precursor ions by collision with SAM surface. Our results demonstrate that TFECs indeed become sharper at short reaction times because the fragmentation probability undergoes a very sharp transition from slow decay to sudden death of excited ions and not because of the narrow internal energy distribution of precursor ions. In fact, in agreement with our previous studies on SID of small peptides, we find that internal energy distributions of larger peptides are quasi-thermal.[5,6,9]

Dissociation Parameters. It is interesting to examine dissociation parameters for des-Arg^1- and des-Arg^9-bradykinin obtained from the best fit of experimental TFECs and compare them to dissociation parameters obtained from BIRD experiments[30] (see Table 1). In our recent study[29] we converted Arrhenius activation parameters for des-Arg^1- and des-Arg^9-bradykinin into threshold energies and reaction entropies using Tolman's theorem and absolute reaction rate theory, assuming a temperature of 450 K. We found that, for reactions proceeding via a very tight transition state, Tolman's correction becomes fairly large. The correction becomes smaller when the preexponential factor is in the range from 10^{10} to 10^{17} s^{-1}. The thermal fragmentation of des-Arg^1- and des-Arg^9-bradykinin is characterized by very different preexponential factors of 10^7 and 10^{12} s^{-1}, respectively, which results in Tolman's theorem corrections of 0.33 eV for des-Arg^1-bradykinin and 0.04 eV for des-Arg^9-bradykinin. Thermal data indicates that the two precursor ions have significantly different activation entropies for dissociation. In contrast, our modeling indicates that activation entropies for dissociation of des-Arg^1- and des-Arg^9-bradykinin are very similar, resulting in similar preexponential factors of 4×10^8 and 2×10^8 s^{-1}, respectively.

There is an excellent agreement between dissociation parameters for des-Arg^1-bradykinin extracted from BIRD data and obtained by modeling of time-resolved SID experiments. The dissociation threshold calculated from Arrhenius parameters (1.15 eV) is within the error bar of the threshold energy extracted from our modeling. The preexponential factor obtained in this study (4×10^8 s^{-1}) is somewhat higher than the preexponential factor obtained from BIRD studies (10^7 s^{-1}). Nevertheless, thermal rates calculated by averaging microcanonical rate−energy dependencies, $k(E)$, over thermal distributions at appropriate temperatures show less than 20% deviation from the thermal rate constants reported by Williams and co-workers[30] (see Figure 8).

For des-Arg^9-bradykinin, both the threshold energy (1.09 eV) and the preexponential factor (2×10^8 s^{-1}) are substantially different from the values obtained in thermal experiments (1.24 eV and 10^{12} s^{-1}, respectively). In addition, it has been reported in ref 30 that thermal dissociation of des-Arg^9-bradykinin does not fall in the rapid exchange limit,[34,35] meaning that the experimental Arrhenius parameters are lower than the "high-pressure" parameters. This implies an even larger difference between the thermal data and our modeling results. The deviations between BIRD rate constants and thermal rates calculated on the basis of the microcanonical rate constants, $k(E)$, are quite small (Figure 8). However, our rate constants fall on a line with a significantly different slope and intercept than the BIRD data. It should be noted that extraction of threshold energies and activation entropies from the RRKM modeling is sensitive to the choice of the parameters describing the energy deposition function. However, within the flexibility limits given by the functional form of the energy deposition function utilized in this work, we could not obtain a better match between the BIRD data and our model for des-Arg^9-bradykinin.

We have previously demonstrated that ion−surface impact results in deposition of a quasi-thermal distribution of internal energies in the excited ions.[6] However, there is a significant difference between SID and BIRD experiments. In SID experi-

(34) Dunbar, R. C.; McMahon, T. B. *Science* **1998**, *279*, 197.
(35) Price, W. D.; Williams, E. R. *J. Phys. Chem. A* **1997**, *101*, 8844.

ments the internal energy is deposited instantaneously into the ion, implying that only those conformations that are available at room temperature undergo activation. Following the excitation event the ion ensemble is allowed to relax by dissociation and radiative cooling for a variable reaction time. Ion dissociation after 100 ms is strongly suppressed because of radiative cooling (see Figure 6). In contrast, in BIRD experiments the ion ensemble undergoes radiative activation/deactivation for the entire time of the kinetic experiment, which varies from 30 to 300 s for temperatures ranging from 145 to 200 °C for protonated des-Arg^1- and des-Arg^9-bradykinin. Because dissociation is very slow, excited ions in BIRD experiments explore the available conformational space at temperatures substantially above the room temperature and are likely to isomerize during the time scale of the experiment. After isomerization a different conformation or family of conformations continues the activation/deactivation process prior to fragmentation. We suggest that the differences in dissociation parameters for des-Arg^9-bradykinin derived in this study and deduced from BIRD data result from the differences in conformations of protonated peptides that undergo activation in the two different types of experiments.

Conclusions

Time- and collision energy-resolved SID of des-Arg^1- and des-Arg^9-bradykinin was examined by FT-ICR MS. Collision energy-resolved experiments demonstrated that there is a sharp transition in fragmentation behavior of these ions. At low collision energies (15−25 eV) both ions fragment in a very selective manner and exhibit very few product ions in their SID spectra. Increasing collision energy above 30 eV results in opening of a variety of dissociation pathways, and the number of fragments in the spectrum increases dramatically. Time-resolved studies demonstrated that most of the high-energy fragments could not be attributed to consecutive dissociation of primary fragment ions but are rather formed directly from the excited precursor ion.

RRKM-based modeling of time-resolved fragmentation efficiency curves (TFECs) provided further insights into the nature of dissociation of protonated des-Arg^1- and des-Arg^9-bradykinin. Modeling demonstrated that dissociation of these ions could be adequately described only by assuming two decay rates: slow and fast. Furthermore, the fast decay rate is well represented by the "sudden death" approximation, which assumes that precursor ions fragment instantly following the ion activation event once the internal energy deposited by ion−surface impact exceeds a certain threshold. We suggest that these findings are indicative of a shattering transition, when excited ions fragment during their interaction with a surface. A similar transition has been observed previously for cluster ions[12−18] and predicted for protonated glycine[22] but has never been reported for peptide ions.

The shattering transition has a profound effect on the type and amount of fragments observed in SID spectra, the shapes of fragmentation efficiency curves, and their dependence on the collision energy. At long reaction times, TFECs of both ions are mainly defined by the slow decay processes and the dependence of the parent ion intensity on collision energy is relatively slow. Fast decay is dominant at short reaction times, resulting in much steeper shapes of TFECs. Although the slow decay rate for des-Arg^9-bradykinin is higher than for des-Arg^1-bradykinin, threshold energies for the fast fragmentation pathway for both ions are essentially the same. This is expressed in the time dependence of the collision energies required to observe 50% depletion of the precursor ion, which diverge at longer reaction times and closely approach each other at shorter times. This finding resolves an apparent contradiction noticed in our previous study.[29] Considering only the slow decay rate, fragmentation efficiency curves of des-Arg^1- and des-Arg^9-bradykinin should have diverged quite significantly at short reaction time. This assertion disagreed with the collision energy-resolved study using a tandem-quadrupole setup, in which FECs of these ions perfectly overlapped.[33] Our modeling demonstrats that at 10 μs reaction time (characteristic of the tandem-quadrupole SID experiments) FECs for both ions are determined solely by shattering, which results in the overlap of the curves.

Dissociation parameters for des-Arg^1-bradykinin obtained in this study are in excellent agreement with BIRD results.[30] However, both the dissociation threshold for des-Arg^9-bradykinin and the transition-state entropy obtained for des-Arg^9-bradykinin are lower than the dissociation threshold derived from BIRD data.[29] We attribute this difference to the slow and fast activation of precursor ions in the two classes of experiments. Slow thermal activation and dissociation allows excited ions to explore the conformational space and undergo many isomerizations while continuously activating both the original and the isomeric conformations. In contrast, essentially instant activation by ion−surface impact probes the dissociation of the conformations of precursor ions that strike the surface after having been thermalized in the storage quadrupole section of our apparatus.[25]

Acknowledgment. The research described in this manuscript was performed at the W. R. Wiley Environmental Molecular Sciences Laboratory, a national scientific user facility sponsored by the U.S. Department of Energy's Office of Biological and Environmental Research and located at Pacific Northwest National Laboratory. PNNL is operated by Battelle for the U.S. Department of Energy. Research at EMSL was carried out within Project 40457 supported by the Office of Basic Energy Sciences of the U.S. Department of Energy. T.H.B. thanks the NSF for Grant CHE-9634238 for financial support.

JA027915T